NeuroImage 310 (2025) 121144

Contents lists available at ScienceDirect

NeuroImage

journal homepage: www.elsevier.com/locate/ynimg

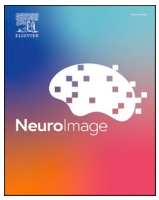

Standardized low-resolution brain electromagnetic tomography does not improve EEG Alzheimer's disease assessment

Wolfgang Frühwirt [a,b,*], Martin Mairhofer [b], Andreas Hahn [c], Heinrich Garn [d], Markus Waser [d], Reinhold Schmidt [e], Thomas Benke [f], Peter Dal-Bianco [g], Gerhard Ransmayr [h], Dieter Grossegger [i], Stephen Roberts [a], Georg Dorffner [b]

[a] Machine Learning Research Group, University of Oxford, Oxford, UK
[b] Institute of Artificial Intelligence, Medical University of Vienna, Vienna, Austria
[c] Department of Psychiatry and Psychotherapy, Medical University of Vienna, Vienna, Austria
[d] AIT Austrian Institute of Technology GmbH, Vienna, Austria
[e] Department of Neurology, Medical University of Graz, Graz, Austria
[f] Department of Neurology, Medical University of Innsbruck, Innsbruck, Austria
[g] Department of Neurology, Medical University of Vienna, Vienna, Austria
[h] Department of Neurology 2, Kepler University Hospital, Linz, Austria
[i] Dr. Grossegger & Drbal GmbH, Vienna, Austria

ARTICLE INFO

Keywords:
3D source localization
Quantitative EEG
Alzheimer's disease
Dementia
sLORETA

ABSTRACT

Quantitative EEG has been shown to reflect neurodegenerative processes in Alzheimer's disease (AD) and may provide non-invasive and widely available biomarkers to enhance the objectivization of disease assessment. To address EEG's major drawback – its low spatial resolution – many studies have employed 3D source localization. However, none have investigated whether this complex mapping into 3D space actually adds value over standard surface derivation. In fact, we found no prior study – in any disease – that quantitatively compared the results of a 3D source localization method with those achieved by surface derivation. We analyzed data from one of the largest prospective AD EEG studies ever conducted (four study centers, 188 patients, 100 female). Thousands of distinct quantitative EEG markers of slowing, complexity, and functional connectivity were computed and regressed against disease severity, with rigorous control for multiple testing. We found highly significant associations between quantitative EEG markers and disease severity. However, standardized low-resolution electromagnetic tomography (sLORETA), a widely used 3D source localization method, did not improve results. Furthermore, a surface derivation marker (auto-mutual information of the left hemisphere during the eyes-closed condition) was the best performing marker across our entire sample. While our findings strongly support that quantitative EEG markers reflect neurodegenerative processes in AD, they do not demonstrate additional benefit from sLORETA. Importantly, our results are specific to AD and sLORETA. Therefore, they should not be generalized to other neurological or psychiatric disorders or to other 3D source localization methods without further validation. Finally, these findings do not diminish the value of 3D source localization for visual EEG inspection.

1. Introduction

AD is a degenerative brain disease and the most common form of dementia. The progressive accumulation of extracellular beta-amyloid plaques and the formation of intracellular neurofibrillary tangles of hyperphosphorylated tau are considered its hallmark pathologies. These changes are accompanied by the damage and destruction of neurons, ultimately leading to the death of the individual (Alzheimer's Association, 2017).

A definitive AD diagnosis can only be obtained through histological analysis of brain tissue, which is normally acquired post-mortem. Possible and probable AD diagnoses (NINCDS-ADRDA) are most commonly based on neuropsychological testing and subjective clinical interpretations, as existing markers with high diagnostic validity are

* Corresponding author at: Machine Learning Research Group, University of Oxford, Eagle House, Walton Well Road, Oxford OX2 6ED, UK.
E-mail address: w.fruehwirt@neurowissenschaften.at (W. Frühwirt).

https://doi.org/10.1016/j.neuroimage.2025.121144
Received 28 August 2024; Received in revised form 28 February 2025; Accepted 13 March 2025
Available online 14 March 2025

invasive and/or costly (e.g., analysis of cerebrospinal fluid; positron emission tomography, PET).

To further objectivize AD diagnosis in routine clinical practice, one would wish for non-invasive, inexpensive, and widely available markers such as those potentially provided by quantitative EEG (QEEG). Therefore, numerous trials have been conducted to investigate the usefulness of QEEG markers for AD assessment (Dauwels et al., 2010a; Jeong, 2004). Many of which have used 3D source localization techniques to mitigate the major drawback of EEG, its low spatial resolution (e.g., Aoki et al., 2023; Cecchetti et al., 2021; Babiloni et al., 2023; Hata et al., 2016; Nishida et al., 2011).

Briefly, 3D EEG source localization methods localize electric activity within the brain (neuronal post-synaptic processes) based on surface electrode recordings. The most prominent method is low-resolution brain electromagnetic tomography (LORETA) (Pascual-Marqui et al., 1994). Assuming that neighboring neurons are simultaneously and synchronously activated, it solves the 'inverse problem', i.e. the localization of electric neuronal activity based on extracranial measurements, by introducing the constraint of maximal synchronization and selects the smoothest of all possible 3D current distributions.

Cross-modality validation studies supporting LORETA have compared its results with structural magnetic resonance imaging (MRI) (Worrell et al., 2000), functional MRI (Mulert et al., 2004; Vitacco et al., 2002), and PET (Zumsteg et al., 2005; Oakes et al., 2004; Pizzagalli et al., 2003). Furthermore, in AD patients, Dierks et al. (2003) have shown that the spatial pattern of cerebral glucose metabolism, as measured by fluorodeoxyglucose PET, correlates with the LORETA localization of intracerebral EEG generators.

However, no AD study has ever investigated the fundamental usefulness of LORETA as compared to standard surface derivation (SURFACE). In fact, we could not find any clinical study – all fields of research considered – that quantitatively compared results of LORETA or similar methods with those achieved by surface derivation.

Using data of one of the largest prospective AD EEG studies ever conducted, we utilize standardized low-resolution brain electromagnetic tomography (sLORETA) (Pascual-Marqui, 2002) to map two-dimensional surface EEG recordings into a 3D representation, allowing for the calculation of source localized signals of specific regions of interest (ROIs) within a patient's brain. sLORETA represents an improvement of the previous LORETA method. It has low spatial resolution but zero localization error in the presence of measurement and biological noise (Pascual-Marqui, 2002). Compared to exact low-resolution brain electromagnetic tomography (eLORETA), sLORETA is more robust, as eLORETA's assumptions about biological noise may not always align with electrophysiological reality, thus limiting its applicability in clinical settings like ours (Pascual-Marqui, 2007).

As it has been shown that particularly measures of EEG slowing, complexity, and functional connectivity are useful for the assessment of AD (Dauwels et al., 2010a; Jeong, 2004), we compute numerous QEEG markers of these categories and then regress them against AD severity, as measured by the Mini-Mental State Examination (MMSE).

Finally, to assess the added value of sLORETA, we compare its results to those obtained by SURFACE. We hypothesize that the variance explained by our models increases when computing QEEG markers from ROIs predominantly affected by AD, as compared to surface electrode signals.

To the best of our knowledge, the present study is not only the first one to statistically compare outcomes of a 3D source localization method to those achieved by SURFACE, but also the study with the largest prospective multi-center AD sample to compare QEEG markers of slowing, complexity, and functional connectivity.

2. Materials and methods

2.1. Participants

The subjects analyzed were participants in the PRODEM (Prospective Dementia Database Austria) study, where AD patients were recruited at the neurological departments of the Medical Universities of Graz, Innsbruck and Vienna, as well as Kepler University Hospital. Answering different research questions, parts of the PRODEM cohort were analyzed in previous studies (Garn et al., 2014a; Garn et al., 2015; Waser et al., 2016; Fruehwirt et al., 2019), where acquisition and data pre-processing methods are detailed.

Inclusion criteria were (i) diagnosis of Alzheimer-type dementia (NINCDS-ADRDA criteria), (ii) minimum age 40 years, (iii) non-institutionalization and no need for 24-hour care, (iv) availability of a caregiver who provides information on the patient's condition. The inability to sign an informed consent form and the existence of comorbidities likely to preclude the termination of the study were considered exclusion criteria.

Participants were categorized as having 'possible' or 'probable' Alzheimer's disease according to the NINCDS-ADRDA criteria. This classification is widely used in the domain relevant to this study and aligns with prior research, including the studies referenced in this manuscript and our own foundational work, to ensure consistency and comparability across the literature.

The ethics committee of each participating institution approved PRODEM and all participants gave their written informed consent.

Only participants with complete clinical information (level of education, duration of illness, MMSE score, anti-dementia medication, age) and at least 120 s of artifact-free EEG data for each analyzed recording condition were considered.

Demographic and clinical characteristics of the participants are shown in Table 1.

Table 1
Demographic and clinical characteristics of subjects.

	All	Probable AD	Possible AD
Number of subjects	188	133	55
Center 1	57	48	9
Center 2	39	32	7
Center 3	64	33	31
Center 4	28	20	8
Females	100	70	30
Age (years)	74.86 ± 8.06 SD	73.72 ± 8.18 SD	77.60 ± 7.10 SD
Education (years)	11.14 ± 3.04 SD	11.30 ± 3.07 SD	10.74 ± 2.95 SD
Duration of illness (months)	26.88 ± 24.11 SD	27.49 ± 25.78 SD	25.41 ± 19.64 SD
Anti-dementia medication	115 (61.17%)	85 (63.91%)	30 (54.55%)

AD: Alzheimer's disease; Center 1 = Medical University of Graz, Department of Neurology; Center 2 = Medical University of Vienna, Department of Neurology; Center 3 = Medical University of Innsbruck, Department of Neurology; Center 4 = Kepler University Hospital, Department of Neurology 2; MMSE: Mini-Mental State Examination; Mean values ± standard deviations.

2.2. EEG recording

EEG data were acquired according to a rigorously standardized protocol as part of the PRODEM study to ensure consistency, enhance data quality, and minimize inter-center variability.

Patients sat on a comfortable chair with a neck rest. Nineteen gold cup electrodes were placed according to the 10–20 system and impedance levels were kept below 10 kΩ. The electrodes were referenced to connected mastoids, the ground positioned at FCz. EEG was recorded during two resting states, i.e., eyes-closed condition (EC, 360 s), and eyes-open condition (EO, 360 s). The electrooculogram (EOG) was recorded from electrodes by the left and right outer cantus (horizontal EOG) and from electrodes above and below the left eye (vertical EOG). Wrist clip electrodes acquired an electrocardiogram (ECG).

The same amplifier model (AlphaEEG, alpha trace medical systems, Vienna, Austria) and software were used across all study centers. The amplifier applied a 0.3–70 Hz band-pass filter and a 50 Hz notch filter to the signal. Digitization was conducted at 256 Hz with 16 bit resolution. Operators received standardized training, and compliance with the protocol was ensured through close supervision.

2.3. EEG preprocessing

We individually identified and manually excluded EEG segments which were affected by artifacts in a way that could not be corrected by other methods (e.g., electrode "pops"). To eliminate low-frequency artifacts from transpiration, data was highpass-filtered at a cutoff frequency of 2 Hz using a stable, direct-form finite impulse response (FIR) filter with linear phase and order 340. ECG artifacts were detected and corrected using a modified energy interval histogram method (Park et al., 2002) and a modified Pan-Tompkins algorithm (Waser and Garn, 2013). Eye movement artifacts were corrected by lowpass-filtering (12 Hz) both EOG channels and regressing them to the EEG channels (Draper and Smith, 2014).

After rejection and correction of artifacts the EEG was analyzed in blocks of 1024 samples (4 s) with 512 samples overlap (2 s). To decrease intersubject variability, only the first 30 artifact-free blocks (120 s) per patient and condition were used for any given computation. An augmented Dickey–Fuller test verified the stationarity of the segmented signal at a 4-sec block length (Dickey and Fuller, 1979a).

To enhance consistency across centers, all EEG data were processed centrally.

2.4. 3D source localization with sLORETA

sLORETA analyses were based on the MNI152 template (Mazziotta et al., 2001). Here, the Talairach Atlas (Lancaster et al., 2000), a coordinate-based system to retrieve brain labels, was used to restrict

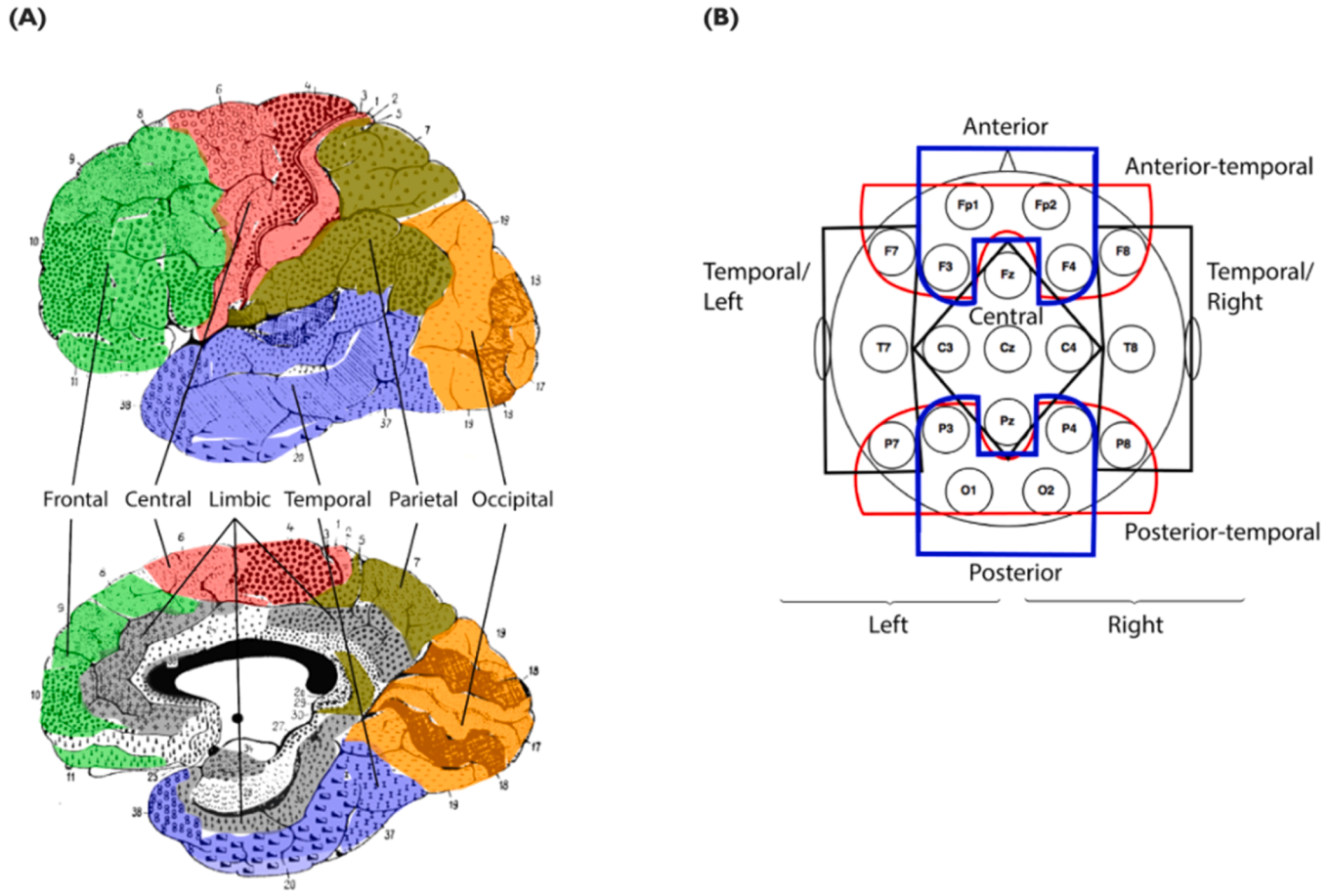

Fig. 1. Arrangement of Definition 1 of sLORETA regions of interest and surface electrode clusters.
(A) Arrangement of Definition 1 of the sLORETA regions of interest (ROIs) based on Brodmann areas according to Babiloni et al. (2017) and Babiloni et al. (2016), subdivided into left (L) hemisphere and right (R) hemisphere. Frontal/L.:8L, 9L, 10L, 11L, 44L, 45L, 46L, 47L; Frontal/R.: 8R, 9R, 10R, 11R, 44R, 45R, 46R, 47R; Central/L.: 1L, 2L, 3L, 4L, 6L; Central/R.: 1R, 2R, 3R, 4R, 6R; Temporal/L.: 20L, 21L, 22L, 37L, 38L, 41L, 42L; Temporal/R.: 20R, 21R, 22R, 37R, 38R, 41R, 42R; Parietal/L. 5L, 7L, 30L, 39L, 40L, 43L; Parietal/R.: 23R, 24R; Limbic/L.: 31L, 32L, 33L, 34L, 35L, 36L; Limbic/R.: 31R, 32R, 33R, 34R, 35R, 36R; Occipital/L.: 17L, 18L, 19L; Occipital/R.; 17R, 18R, 19R; Left: 1L to 11L, 17L to 22L, 30L to 47L; Right: 1R to 11R, 17R to 22R, 30 to 47R. **(B)** Arrangement of surface electrode clusters according to Dauwels et al. (2010b) and Garn et al. (2015) sLORETA: Standardized low-resolution brain electromagnetic tomography; SURFACE: standard surface derivation.

measured neuronal activity to grey matter located at cortical and hippocampal areas. sLORETA includes a correction to account for differences between MNI and Talairach brain templates (Brett et al., 2002). Under these neuroanatomical constraints a total of 6239 voxels with a spatial resolution of 5 mm was available for analysis.

2.5. Quantitative EEG markers

As there exists no commonly agreed upon definition of brain areas to be considered for LORETA analysis in AD, we investigated several variants. First, we used the arrangement of ROIs by Babiloni et al. (2016) and Babiloni et al. (2017). Note that we segmented into left and right hemispheres for a more detailed breakdown and better comparability with SURFACE results (ROI definition 1, see Fig. 1A). Furthermore, we investigated three additional definitions of ROIs built on histological and neuroimaging studies investigating neuronal effects of AD (Arnold et al., 1991; Delacourte et al., 1999; Valotassiou et al., 2015). See ROI definitions 2, 3, and 4 in Supplementary Table 1. In all four definitions, multiple Brodmann areas (BA) were combined to form 3D clusters, i.e., ROIs in cortical source space.

To compare results achieved by sLORETA with those of SURFACE, surface EEG channels were clustered as in Garn et al. (2015) (see Fig. 1B), who utilized a refined definition of the one by Dauwels et al. (2010b). The specific QEEG markers used in the present study are those established in our prior work (Garn et al., 2014a; Garn et al., 2014b; Garn et al., 2015; Waser et al., 2016). Their rationale is grounded in landmark contributions by Jeong (2004) and Dauwels et al. (2010a, 2010b), which demonstrated that EEG slowing, complexity, and functional connectivity are key domains for understanding neurodegenerative processes in AD.

Table 2 summarizes all the measures of EEG slowing, complexity, and functional connectivity and the respective frequency bands computed.

The phenomenon of EEG slowing was assessed by markers of absolute and relative bandpower as well as the centroid frequency of the periodogram.

For measuring complexity we used three information theoretic measures. Shannon entropy (Shannon, 1948) and Tsallis entropy (Tsallis, 1988) measure the uncertainty and therefore the degree of predictability of a random variable, whereas auto-mutual information represents the mutual information between a time series and its time-delayed version (Cover and Thomas, 1991). The more complex a process, the steeper the decline of its auto-mutual information over time.

To quantify the degree of functional connectivity between brain regions, linear and non-linear measures of dependence (also referred to as measures of synchrony) were utilized. Coherence (magnitude-squared coherence) was computed using the cross-spectral and auto-spectral densities of the signals considered (Rosenberg et al., 1989). Phase coherence was used to estimate phase synchronization between signals.

In order to remove the effect of indirect dependencies between signals, partial coherence was computed as well (Brillinger, 1981). The use of a Parzen window guaranteed for the positive (semi)definiteness of the spectral density estimate and therefore the premised invertibility of the matrices representing cross-spectral and auto-spectral densities. However, none of the coherence measures used accounts for non-linear dynamics, nor can the direction of the quantified relationship be inferred.

Granger causality allows the detection of the strength and direction of dependencies, whereas conditional Granger causality additionally removes the influence of other signals on the relationship investigated (Granger, 1969). Autoregressive coefficients were estimated using the Yule-Walker equations (Yule, 1927; Walker, 1931). The model order was dynamically determined using the Akaike Information Criterion (Akaike, 1974) to balance model fit with parsimony. The degree of Granger causality between clusters was calculated using the Euclidean norm of the autoregressive coefficients across all lags. EEG stationarity was verified using the augmented Dickey-Fuller test (Dickey and Fuller, 1979b), and the signals were divided into 4-second quasi-stationary segments with a 2-second overlap to ensure stability for time-series modeling.

Canonical correlation is based on the eigenvalues of the auto-covariance and cross-covariance matrices and finds linear combinations between signals that have maximal correlation with each other (Hotelling, 1936). Instead of covariance in the time domain, dynamic canonical correlation is based on auto-spectra and cross-spectra, i.e., the frequency domain, and can therefore be considered a generalization of the time-static version of canonical correlation (Brillinger, 1981). Static and dynamic canonical correlation coefficients were derived from the estimated covariance and spectral density using eigen-decomposition

Table 2
Measures of EEG slowing, complexity, and functional connectivity for specific frequency bands.

Phenomenon	Measure	Frequency band
Slowing	Absolute Band Power	2–4 Hz (Delta) 4–8 Hz (Theta) 8–13 Hz (Alpha) 12–20 Hz (Beta1) IAF to IAF +2 Hz (iUA)
	Relative Band Power	2–4 Hz (Delta) 4–8 Hz (Theta) 8–13 Hz (Alpha) 12–20 Hz (Beta1) IAF to IAF +2 Hz (iUA)
	Centroid Frequency	2–20 Hz (Delta-Beta1)
Reduced Complexity	Auto-mutual Information	2–15 Hz (Delta-Beta0)
	Shannon Entropy	2–15 Hz (Delta-Beta0)
	Tsallis Entropy	2–15 Hz (Delta-Beta0)
Perturbed Functional Connectivity	Coherence	2–4 Hz (Delta) 4–8 Hz (Theta) 8–13 Hz (Alpha) 12–15 Hz (Beta0) IAF to IAF +2 Hz (iUA)
	Phase Coherence	2–4 Hz (Delta) 4–8 Hz (Theta) 8–13 Hz (Alpha) 12–15 Hz (Beta0) IAF to IAF +2 Hz (iUA)
	Partial Coherence	2–4 Hz (Delta) 4–8 Hz (Theta) 8–13 Hz (Alpha) 12–15 Hz (Beta0) IAF to IAF +2 Hz (iUA)
	Granger Causality	2–15 Hz (Delta-Beta0)
	Conditional Granger Causality	2–15 Hz (Delta-Beta0)
	Canonical Correlation	2–15 Hz (Delta-Beta0)
	Dynamic Canonical Correlation	2–4 Hz (Delta) 4–8 Hz (Theta) 8–13 Hz (Alpha) 12–15 Hz (Beta0) IAF to IAF +2 Hz (iUA)
	Cross-mutual Information	2–15 Hz (Delta-Beta0)

procedures. The Euclidean norm of these canonical correlation coefficients was used as the synchrony marker.

In contrast to all of the previous measures of functional connectivity, cross-mutual information also factors in non-linear interdependencies. It measures the mutual dependence between two signals, i.e., the amount of information obtained about one signal through the observation of the other one (Shannon and Weaver, 1949). Joint and marginal probability distribution functions were estimated using a joint data histogram with a 10×10 grid of bins. We used the normalized version of cross-mutual information as proposed by Maes et al. (1997).

Further details on parameterization and precise mathematical definitions of all non-conventional measures are comprehensively documented in our prior publications (Waser et al., 2016; Garn et al., 2014b) and the foundational study by Dauwels et al. (2010b).

2.6. Statistical analysis

Potential associations between QEEG markers and MMSE scores were established using linear least-squares regression and quantified by the coefficient of determination (R^2). Analyses were adjusted for the patient's age, the duration of illness, and the years of education as covariates.

Significant differences between coefficients of determination (sLORETA versus SURFACE) were determined by a dependent z-test after square root and Fisher's r-to-z transformations.

We applied the Benjamini-Hochberg (Benjamini and Hochberg, 1995) procedure to control the false discovery rate (FDR) and address the multiple testing problem. This approach controls the expected proportion of false positives (Type I errors) among the rejected hypotheses, providing a balance between error control and statistical power.

To enhance statistical power, minimize variability from small sample sizes, and ensure generalizable findings, we pooled data across all participating centers. This approach mitigates the risk of spurious results when analyzing numerous markers in relatively small single-center cohorts and addresses potential imbalances in sample sizes among centers. Pooling the data thus provides a robust, statistically sound basis for interpretation

All computations and statistical analyses were run in Matlab (Mathworks, Natick, USA).

3. Results

In the following, we report the best performing QEEG marker for each measure of slowing, complexity, and functional connectivity. To illustrate potential differences between patients with probable and possible AD, results for respective subgroups are reported in addition to those of the whole group of AD patients.

3.1. All AD patients

Table 3 reports the coefficients of determination for the group of all AD patients ($N = 188$). Overall, auto-mutual information for the left SURFACE cluster during EC exhibited the highest coefficient of determination ($R^2 = 0.30$, $p = 1.39E\text{-}13$). Fig. 2A depicts the corresponding scatterplot. The negative slope of the regression line indicates that higher auto-mutual information (lower complexity) is associated with lower MMSE scores and therefore higher cognitive impairment. The best marker other than based on auto-mutual information was relative theta bandpower ($R^2 = 0.29$, $p = 6.17E\text{-}13$, EC, left SURFACE cluster). The sLORETA marker with the strongest relation to the MMSE score was dynamic canonical correlation between the left prefrontal ROI and the left cingulate ROI (ROI definition 3) in the individual upper alpha (iUA) frequency band during EC ($R^2 = 0.27$, $p = 6.14E\text{-}12$). Also, the best SURFACE marker of functional connectivity was based on dynamic canonical correlation of iUA, but with a lower R^2value (0.24, $p = 3.35E\text{-}10$, EO, anterior-posterior) than for sLORETA.

Relative bandpower ($R^2 = 0.21$, $p = 5.47E\text{-}9$, beta1, EO, prefrontal/right, ROI definition 2) and Tsallis entropy ($R^2 = 0.14$, $p = 8.68E\text{-}6$, EO,

Table 3
Markers with highest R^2 values for all Alzheimer's disease patients.

	Measure	Frequency	Condition	ROI definition	ROI/ Cluster	R2	p-value
sLORETA	Dynamic Canonical Correlation	iUA	EC	3	Prefrontal/L.-Cingulate/L.	0.27	6.14E-12
	Relative Band Power	beta1	EO	2	Prefrontal/R.	0.21	5.47E-9
	Center Frequency	2–15 Hz	EO	2	Prefrontal/R.	0.16	1.95E-6
	Partial Coherence	beta0	EO	1	Central/R.-Limbic/L.	0.15	3.91E-6
	Phase Coherence	iUA	EC	3	Frontal/L.-Cingulate/L.	0.15	5.37E-6
	Tsallis Entropy	2–15 Hz	EO	4	Frontal/R.	0.14	8.68E-6
	Shannon Entropy	2–15 Hz	EO	4	Frontal/R.	0.14	1.14E-5
	Auto-mutual Information	2–15 Hz	EO	1	Limbic/R.	0.14	1.22E-5
	Absolute Band Power	delta	EC	4	Frontal/R.	0.14	1.27E-5
	Coherence	theta	EO	1	Central/R.-Parietal/R.	0.14	1.28E-5
	Cross-mutual Information	2–15 Hz	EC	1	Parietal/R.-Temporal/R.	0.14	1.96E-5
	Granger Causality	2–15 Hz	EO	1	Parietal/R.-Central/R.	0.14	2.06E-5
	Conditional Granger Causality	2–15 Hz	EC	2	Hippocampal/R.-Angulate/L.	0.13	2.42E-5
	Canonical Correlation	2–15 Hz	EC	4	Frontal/L.-Laterotemporal./R.	0.10	2.78E-4
SURFACE	Auto-mutual Information	2–15 Hz	EC	n.a.	Left	0.30	1.39E-13
	Relative Band Power	theta	EC	n.a.	Left	0.29	6.17E-13
	Centroid Frequency	2–20 Hz	EC	n.a.	Temporal/L.	0.28	1.63E-12
	Dynamic Canonical Correlation	iUA	EO	n.a.	Anterior-Posterior	0.24	3.35E-10
	Cross-mutual Information	2–15 Hz	EC	n.a.	Posterior-Temporal/R.	0.23	7.10E-10
	Partial Coherence	delta	EC	n.a.	Anterior-Posterior	0.21	8.03E-9
	Granger Causality	2–15 Hz	EC	n.a.	Anterior-Temporal/R.	0.16	1.19E-6
	Absolute Band Power	theta	EO	n.a.	Temporal/L.	0.16	1.91E-6
	Tsallis Entropy	2–15 Hz	EO	n.a.	Posterior	0.15	3.96E-6
	Shannon Entropy	2–15 Hz	EO	n.a.	Posterior	0.15	6.54E-6
	Canonical Correlation	2–15 Hz	EO	n.a.	Posterior-Temporal/R.	0.14	9.68E-6
	Conditional Granger Causality	2–15 Hz	EC	n.a.	Anterior-Temporal/R.	0.13	2.89E-5
	Phase Coherence	alpha	EC	n.a.	Central-Temporal/L.	0.13	3.05E-5
	Coherence	beta0	EO	n.a.	Posterior-Temporal/L.	0.13	3.59E-5

Coefficient of determination (R^2) adjusted for the patient's age, the duration of illness, and the years of education. p-value corrected for multiple testing. EC: eyes-closed condition, EO: eyes-open condition, ROI: region of interest, L: left, R: right, iUA: individual upper alpha. sLORETA: Standardized low-resolution brain electromagnetic tomography; SURFACE: standard surface derivation.

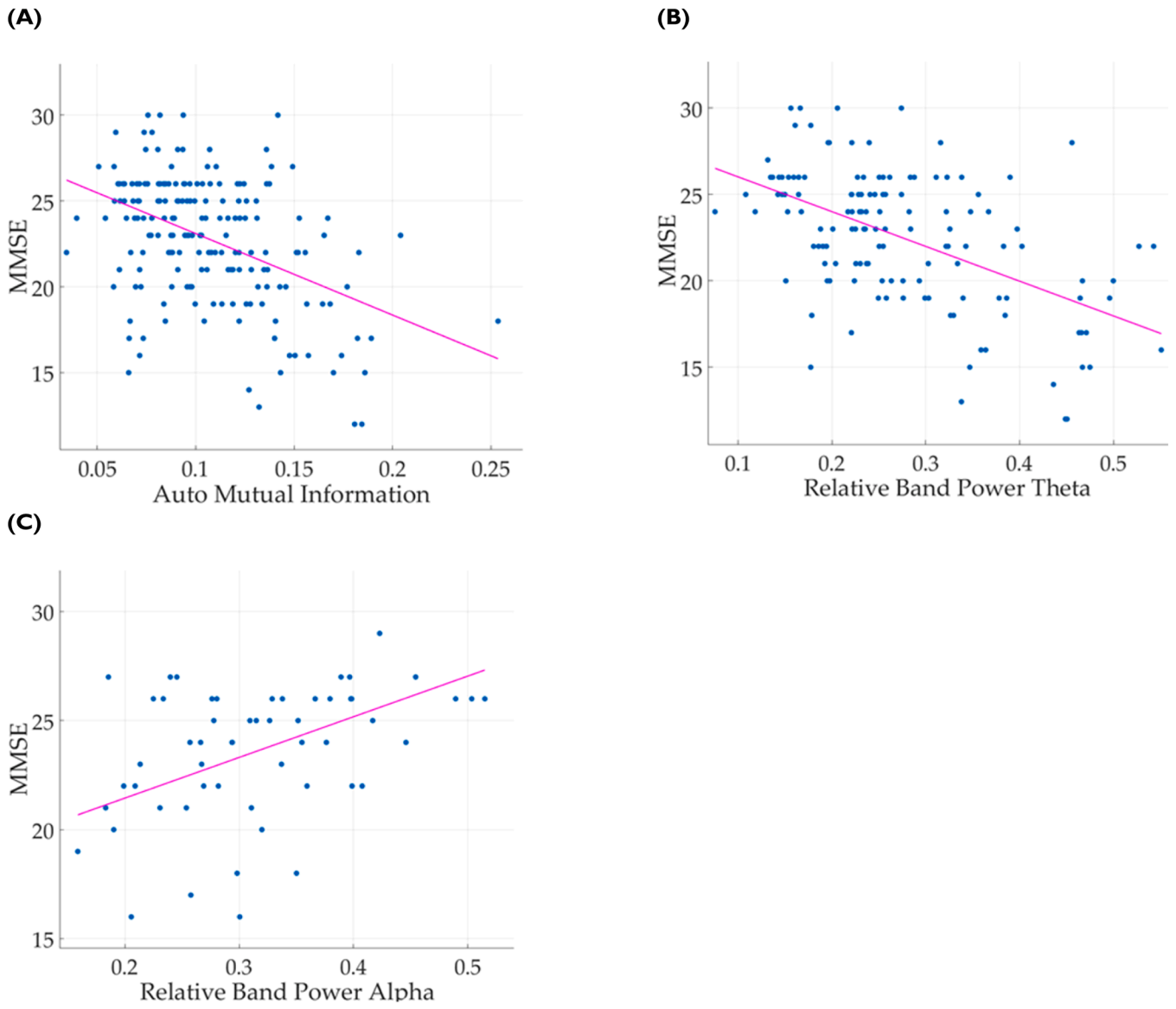

Fig. 2. Scatterplots with fitted regression lines for the marker with highest R^2 value per patient group.
(A) Marker with the highest R^2 value for the group of all Alzheimer's disease patients (auto-mutual information, eyes-closed condition, left hemisphere surface electrode cluster). **(B)** Marker with the highest R^2 value for the group of probable Alzheimer's disease patients (relative theta band power, eyes-closed condition, left hemisphere surface electrode cluster). **(C)** Marker with the highest R^2 value for the group of possible Alzheimer's disease patients (relative alpha band power, eyes-open condition, right temporal surface electrode cluster). MMSE: Mini-Mental State Examination.

frontal/right, ROI definition 4) were the best sLORETA markers of slowing and complexity. All p-values of the QEEG markers reported in Table 3 were significant.

When comparing results between sLORETA and SURFACE, sLORETA performed better for functional connectivity, whereas SURFACE achieved higher R^2 values for slowing and complexity. However, none of the comparisons was significant (Supplementary Table 2).

3.2. Probable AD patients

Results for the group of Probable AD patients ($N = 133$) can be obtained from Table 4. Regression analysis determined that the highest amount of variance was explained by relative theta band power of the left SURFACE cluster ($R^2 = 0.36$, $p = 6.26E\text{-}12$, EC, Fig. 2B).

Auto-mutual information of the left SURFACE cluster ($R^2 = 0.34$, $p = 9.08E\text{-}11$, EC) was the best marker other than relative theta band power markers.

Like in the group of all AD patients, the sLORETA marker with the strongest relation to the MMSE score was dynamic canonical correlation between the left prefrontal ROI and the left cingulate ROI (ROI definition 3) in the iUA frequency band during EC ($R^2 = 0.29$, $p = 4.53E\text{-}9$). It was the marker with the highest R^2value for a functional connectivity marker overall. The best SURFACE connectivity marker was cross-mutual information ($R^2 = 0.27$, $p = 4.82E\text{-}8$, 2–15 Hz, EC, posterior-temporal/left). The leading sLORETA markers for slowing, and complexity were beta1 relative bandpower ($R^2 = 0.21$, $p = 4.06E\text{-}6$, prefrontal/right, ROI definition 2), and auto-mutual information ($R^2 = 0.13$, $p = 1.25E\text{-}03$, temporal/right, ROI definition 2).

Not a single comparison of QEEG markers between modalities yielded a significant result (Supplementary Table 2).

3.3. Possible AD patients

Table 5 shows the markers with the highest coefficients of determination for sLORETA and SURFACE for the group of possible AD patients ($N = 55$).

Table 4
Markers with highest R^2 values for Probable Alzheimer's disease patients.

	Measure	Frequency	Condition	ROI definition	ROI/ Cluster	R2	p-value
sLORETA	Dynamic Canonical Correlation	iUA	EC	3	Prefrontal/L.-Cingulate/L.	0.29	4.53E-9
	Relative Band Power	beta1	EO	2	Prefrontal/R.	0.21	4.06E-6
	Granger Causality	2–15 Hz	EO	1	Central/L.-Limbic/R.	0.17	9.28E-5
	Centroid Frequency	2–20 Hz	EO	2	Temporal/R.	0.16	1.13E-4
	Partial Coherence	delta	EO	4	Frontal/L.-Frontal/R.	0.16	1.70E-4
	Coherence	theta	EO	1	Central/L.-Parietal/R.	0.15	2.30E-4
	Conditional Granger Causality	2–15 Hz	EO	1	Central/L.-Temporal/R.	0.15	3.07E-4
	Phase Coherence	beta0	EO	1	Central/R.-Temporal/R.	0.14	7.00E-4
	Auto-mutual Information	2–15 Hz	EO	2	Temporal/R.	0.13	1.25E-3
	Cross-mutual Information	2–15 Hz	EO	2	Hippocampal/R.-Temporal/R.	0.12	2.71E-3
	Tsallis Entropy	2–15 Hz	EO	4	Frontal/R.	0.12	2.72E-3
	Shannon Entropy	2–15 Hz	EC	1	Occipital/L.	0.12	2.91E-3
	Absolute Band Power	theta	EC	1	Central/L.	0.11	5.51E-3
	Canonical Correlation	2–15 Hz	EO	3	Temporal/R.-Cingulate/R.	0.09	1.42E-2
SURFACE	Relative Band Power	theta	EC	n.a.	Left	0.36	6.26E-12
	Auto-mutual Information	2–15 Hz	EC	n.a.	Left	0.34	9.08E-11
	Center Frequency	2–15 Hz	EC	n.a.	Temporal/L.	0.32	2.87E-10
	Cross-mutual Information	2–15 Hz	EC	n.a.	Posterior-Temporal/L.	0.27	4.82E-8
	Dynamic Canonical Correlation	iUA	EO	n.a.	Anterior-Posterior	0.26	7.82E-8
	Partial Coherence	delta	EC	n.a.	Anterior-Posterior	0.24	3.46E-7
	Granger Causality	2–15 Hz	EC	n.a.	Anterior-Temporal/R.	0.17	6.25E-5
	Tsallis Entropy	2–15 Hz	EO	n.a.	Posterior-Temporal	0.15	3.70E-4
	Absolute Band Power	theta	EO	n.a.	Temporal/L.	0.15	4.12E-4
	Canonical Correlation	2–15 Hz	EO	n.a.	Posterior-Temporal/R.	0.14	6.39E-4
	Shannon Entropy	2–15 Hz	EO	n.a.	Posterior-Temporal	0.14	7.28E-4
	Conditional Granger Causality	2–15 Hz	EO	n.a.	Anterior-Temporal/R.	0.13	9.97E-4
	Phase Coherence	theta	EC	n.a.	Anterior-Temporal/L.-Posterior-Temporal./L.	0.13	1.31E-3
	Coherence	beta0	EO	n.a.	Posterior-Temporal/L.	0.12	1.90E-3

Coefficient of determination (R^2) adjusted for the patient's age, the duration of illness, and the years of education. p-value corrected for multiple testing. EC: eyes-closed condition, EO: eyes-open condition, ROI: region of interest, L: left, R: right, iUA: individual upper alpha. sLORETA: Standardized low-resolution brain electromagnetic tomography; SURFACE: standard surface derivation.

Table 5
Markers with highest R^2 values for Possible Alzheimer's disease patients.

	Measure	Frequency	Condition	ROI definition	ROI/ Cluster	R2	p-value
sLORETA	Coherence	iUA	EC	1	Frontal/R.-Limbic/L.	0.41	2.06E-5
	Absolute Band Power	delta	EC	4	Laterotemporal./R.	0.40	3.44E-5
	Partial Coherence	alpha	EO	3	Prefrontal/R.-Cingulate/L.	0.38	5.79E-5
	Granger Causality	2–15 Hz	EC	1	Frontal/R.-Occipital/L.	0.38	6.15E-5
	Conditional Granger Causality	2–15 Hz	EC	3	Frontal/R.-Cingulate/R.	0.38	7.91E-5
	Phase Coherence	delta	EC	3	Prefrontal/L.-Cingulate/L.	0.36	1.20E-4
	Dynamic Canonical Correlation	delta	EC	3	Frontal/R.-Cingulate/R.	0.33	3.74E-4
	Cross-mutual Information	2–15 Hz	EC	1	Parietal/R.-Limbic/R.	0.32	5.01E-4
	Relative Band Power	iUA	EC	1	Parietal/R.	0.32	6.37E-4
	Auto-mutual Information	2–15 Hz	EC	1	Limbic/R.	0.31	9.50E-4
	Tsallis Entropy	2–15 Hz	EO	1	Frontal/R.	0.30	1.15E-3
	Shannon Entropy	2–15 Hz	EO	1	Frontal/R.	0.29	1.35E-3
	Centroid Frequency	2–20 Hz	EC	1	Occipital/R.	0.24	7.19E-3
	Canonical Correlation	2–15 Hz	EC	2	Prefrontal/L.-Prefrontal/R.	0.23	1.11E-2
SURFACE	Relative Band Power	alpha	EO	n.a.	Temporal/R.	0.45	4.90E-6
	Auto-mutual Information	2–15 Hz	EO	n.a.	Posterior	0.35	2.02E-4
	Centroid Frequency	2–20 Hz	EO	n.a.	Posterior	0.33	3.66E-4
	Cross-mutual Information	2–15 Hz	EO	n.a.	Posterior-Temporal/R.	0.32	5.41E-4
	Partial Coherence	theta	EO	n.a.	Central-Temporal/R.	0.31	8.58E-4
	Absolute Band Power	theta	EO	n.a.	Anterior-Temporal	0.29	1.74E-3
	Conditional Granger Causality	2–15 Hz	EC	n.a.	Temporal/R.-Posterior	0.28	1.93E-3
	Phase Coherence	beta0	EC	n.a.	Anterior-Central	0.28	2.42E-3
	Coherence	alpha	EO	n.a.	Central-Temporal/R.	0.28	2.52E-3
	Dynamic Canonical Correlation	iUA	EC	n.a.	Posterior-Temporal/L.	0.27	2.64E-3
	Canonical Correlation	2–15 Hz	EC	n.a.	Central-Posterior	0.24	6.97E-3
	Granger Causality	2–15 Hz	EO	n.a.	Temporal/R.-Central	0.23	8.57E-3
	Shannon Entropy	2–15 Hz	EO	n.a.	Posterior	0.22	1.19E-2
	Tsallis Entropy	2–15 Hz	EO	n.a.	Posterior	0.22	1.20E-2

Coefficient of determination (R^2) adjusted for the patient's age, the duration of illness, and the years of education. p-value corrected for multiple testing. EC: eyes-closed condition, EO: eyes-open condition, ROI: region of interest, L: left, R: right, iUA: individual upper alpha. sLORETA: Standardized low-resolution brain electromagnetic tomography; SURFACE: standard surface derivation.

Relative alpha bandpower ($R^2 = 0.45$, $p = 4.90E\text{-}6$, SURFACE, EO, temporal/right) was the marker with the maximal association with MMSE scores overall (Fig. 2C).

The highest R^2value (0.41, $p = 2.06E\text{-}05$) for a functional connectivity marker was obtained by a sLORETA marker (coherence, iUA, EC, frontal/right-limbic/left, ROI definition 1). It was the best marker other than based on relative alpha band power. For SURFACE the leading markers of complexity, and functional connectivity were auto-mutual information ($R^2 = 0.35$, $p < 2.02E\text{-}04$, EO, posterior), and cross-mutual information ($R^2 = 0.32$, $p < 5.41E\text{-}04$, EO, posterior-temporal/right). The premier sLORETA markers of slowing, and complexity were absolute delta band power ($R^2 = 0.40$, $p < 3.44E\text{-}05$, EC, lateroteporal/right, ROI definition 4), and auto-mutual information ($R^2 = 0.31$, $p < 9.50E\text{-}04$, EC, limbic/right, ROI definition 1).

There were no statistically significant differences between sLORETA and SURFACE markers (Supplementary Table 2).

4. Discussion

To examine the potential advantages of 3D source localization, results achieved by sLORETA were compared to those obtained by standard referential derivation. In total, 9254 QEEG markers were analyzed (sLORETA, 8434; SURFACE, 820).

Various QEEG measures of slowing, loss of complexity, and perturbation of functional connectivity – which are thought to be associated with the death of cortical neurons, axonal pathology, cholinergic deficits, and resulting functional disconnections between cortical areas in AD (Jeong, 2004) – were highly significantly related to disease severity, demonstrating their general usefulness.

In all patient groups analyzed, SURFACE markers achieved the highest coefficients of determination when considering all types of QEEG measures. Broken down into categories of EEG measures, SURFACE markers attained higher R^2 values regarding EEG slowing and complexity, whereas the sLORETA technique achieved superior results for functional connectivity. This order was the same for all groups of subjects.

However, none of the comparisons between SURFACE and sLORETA outcomes was significant. Hence, our hypothesis that the variance explained by our models would significantly increase when computing QEEG markers from ROIs predominantly affected by AD, as compared to surface electrode signals, was not confirmed.

Over the entire group of subjects, the best QEEG marker of AD severity was based on auto-mutual information. Auto-mutual information was not only top of the list for the combined sample when considering all categories of markers, but also ranked highest in the category of complexity markers in both sub-samples of patients. Our results therefore further emphasize the importance of the loss of EEG complexity in neurodegenerative diseases, as previously described in the scientific literature (Dauwels et al., 2010a; Jeong, 2004). The computation of information theoretic measures capturing nonlinear, dynamic information processing in the brain – especially in the left hemisphere – seems to be particularly useful.

Considering the entire sample of subjects, the second best QEEG marker overall was the relative band power in the theta rage, which also explained the highest amount of variance of all markers in the group of probable AD patients (both at the left-hemispheric cluster of electrodes). Also this result is well in line with previous reports. For instance, Dauwels et al. (2010b) showed that theta band relative power is significantly larger in AD patients compared to age-matched control subjects, and allows for the best distinction between groups out of all QEEG measures investigated. Notably, in the same study Dauwels and colleagues demonstrated a strong correlation between theta relative power and complexity markers – potentially explaining the similarity of outcomes for these measures in our own investigation. The rationale for the relationship between these phenomena is that low-frequency EEG signals are more regular than signals with high-frequency components, and therefore exhibit characteristics of reduced complexity.

Regarding functional connectivity, sLORETA markers explained the highest amount of variance of MMSE scores. Notably, the top-ranking sLORETA markers of all patient groups were based on iUA. A number of frameworks suggest that alpha amplitude modulations play a crucial role in the inhibitory control and timing of cortical processing, thereby allocating neuronal resources properly and preventing task-irrelevant activities from interfering with memory processes (Hanslmayr et al., 2012; Jensen and Mazaheri, 2010; Klimesch et al., 2007).

Especially the iUA band has been related to memory performance (Klimesch, 1999; Klimesch et al., 2006; Pfurtscheller and Aranibar, 1977) – which corresponds to our results. Dynamic canonical correlation ranked highest in the groups of all AD patients, as well as probable AD patients, whereas magnitude-squared or ordinary coherence was the premier marker in the possible AD sample. Notably, both of these measures are based on cross-spectral and auto-spectral densities, i.e., using the frequency domain instead of the time domain, and are therefore resistant to phase differences between signals. Both, for the entire group of subjects as well as for the group of probable AD subjects the best markers of functional connectivity measured the coactivity between prefrontal and cingulate regions (prefrontal/left-cingulate/left, ROI definition 3). While all of the constituent BAs of the respective ROIs have been shown to be histologically altered in AD (Arnold et al., 1991), the cingulate ROI definition used corresponds quite well to the areas of the midline core component (Andrews-Hanna et al., 2010) of the default mode network (DMN), whereas the prefrontal ROI encompasses many areas of the fronto-parietal network (Palmqvist et al., 2017). Palmqvist et al. (2017) showed that both intra-DMN as well as DMN-FPN functional connectivity is associated with cerebrospinal fluid beta-amyloid 42 levels, a prime AD biomarker (Hampel et al., 2018).

One could speculate that the higher R^2 values achieved by sLORETA compared to SURFACE regarding functional connectivity in all groups of patients might be due to the ability of source derivation techniques to ameliorate the volume conduction artifact. By reducing artificial variance shared between regional signals, sLORETA potentially improves the signal-to-noise ratio and, therefore, the outcome of EEG synchrony measures. For those measures examined that do not consider the interaction between signals, i.e., that of slowing and complexity, the robustness of signals from simple clusters of surface electrodes potentially outweighs the advantage of the improved spatial restriction of signals of sLORETA. However, these considerations are purely speculative, as none of the differences in outcomes between SURFACE and sLORETA were significant.

Testing more than ten times as many sLORETA markers compared to SURFACE markers inherently favored sLORETA due to the increased probability of detecting significant results by chance alone.

The dominance of left hemispheric regions of the premier QEEG markers in our study might be explained by the essential role of language for cognitive processes and the fact that the left cerebral hemisphere is dominant in language processing in the overwhelming majority of humans (Vigneau et al., 2006).

When comparing our best sLORETA results to those of other studies investigating the association between MMSE scores and source derivation QEEG markers, our effect sizes lie in between. Hata et al. (2016) found significant linear correlations (R^2 values of up to 0.26) when using lagged phase coherence of source localized ROIs as measure of functional connectivity. Analyzing LORETA current density in various frequency bands, the results of Gianotti et al. (2007) yielded maximal R^2 values of 0.45. Yet, these calculations were based on 21 subjects only. Mitchell (2009) investigated linear correlations in a combined group of patients with mild cognitive impairment and AD and found R^2 values of up to 0.11. Note that all of the three aforementioned studies had a single-center design.

Having a variety of strengths (e.g., large sample size, multi-center design, standardized acquisition protocol and uniform hardware, broad variety of basic and state-of-the-art QEEG measures), the present

study also has limitations.

For instance, the use of only 19 EEG channels limits our findings. High-density EEG recording would have allowed for a higher spatial resolution. However, we wanted to examine options for an improvement of AD assessment in daily clinical practice in secondary and tertiary neurological care, where the 10–20 system with 19 electrodes is the standard. Furthermore, using the regular number of channels does not necessarily imply mislocation and is common practice in 3D source localization studies in AD (e.g., Shim and Shin (2020), Caso et al. (2012), Nishida et al. (2011), Babiloni et al. (2004), Gianotti et al. (2007), Babiloni et al. (2006a), Babiloni et al. (2006b), Babiloni et al. (2006c), Babiloni et al. (2010), Babiloni et al. (2011), Babiloni et al. (2013), Triggiani et al. (2017), Canuet et al. (2012), Dattola and La Foresta (2020), Babiloni et al., (2017)). Moreover, Dierks et al. (2003), using the standard 10–20 system in patients with AD, showed that the distribution of glucose metabolism on FDG-PET correlates with the equivalent dipole derived from LORETA-based EEG source analysis. Finally, Pascual--Marqui (2002) demonstrated in his seminal sLORETA study that robust source localization can be achieved with a moderate electrode number, supporting the principle that high-density arrays are not strictly required for valid source reconstruction

We used the sLORETA variant of LORETA due to its robustness. eLORETA might yield slightly different results. However, Pascual-Marqui, who developed both methods, notes that eLORETA's assumptions about biological noise "..might have little relation to electrophysiological reality. This might be seen as a disadvantage of eLORETA as compared to sLORETA." (Pascual-Marqui, 2007, p.7). Consequently, we chose sLORETA for our clinical settings. Notably, a new variant, EHR-sLORETA, has recently been proposed, which may provide additional advantages in specific contexts (Sadat-Nejad and Beheshti, 2021).

Since our study design already involved computing thousands of distinct quantitative EEG markers and statistically comparing them between SURFACE and LORETA, we focused on a single, robust, and widely recognized global measure of disease severity – the total MMSE score. This ensures statistical rigor and clarity within our extensive analytic framework. Furthermore, it facilitates straightforward integration of our findings with the large body of AD literature, where the MMSE total score is the most commonly used measure of global cognitive impairment (Mitchell, 2009). Nonetheless, as no 'ultimate' measure of AD severity exists, investigating the relationship between the outcomes of other neuropsychological instruments or subdomain-specific MMSE scores and QEEG markers could provide insights into additional aspects of disease severity.

We did not apply independent component analysis (ICA) or similar techniques that decompose multivariate signals into additive subcomponents. Investigating whether such approaches offer advantages for 3D source localization over surface-based methods represents a valuable avenue for future research.

While our study focused on evaluating individual markers, we recognize that machine learning approaches could capture patterns in the data that may highlight the benefits of sLORETA preprocessing. Moreover, recent efforts to integrate neuropsychological and electrophysiological features – either independently or in combination – through machine learning offer promising directions for further research (Carrarini et al., 2024). Vecchio et al. (2020) demonstrated that combining machine learning with eLORETA aids AD identification, while Maestú et al. (2015) showed that a machine learning approach can accurately identify patients with Mild Cognitive Impairment based on the pattern of functional connectivity measured with magnetoencephalography.

Our regression models controlled for key confounders, specifically age, education, and disease duration, based on their established relevance in AD research. As other potential confounders may exist, future studies could incorporate a broader range of covariates to further strengthen model robustness.

Our study aimed to assess disease severity within AD rather than to distinguish AD from healthy individuals. Including elderly controls in future work would help clarify the specificity of these EEG markers for AD detection.

Furthermore, our study specifically examined sLORETA, and a broader comparison with other source localization methods could be a valuable direction for future research.

Finally, is essential to emphasize that 3D source representations provide anatomically meaningful visualizations that may enhance interpretability. This added clarity can be especially valuable for audiences less familiar with EEG analysis and remains a strength of source-based approaches.

5. Conclusions

Our findings strongly support that QEEG markers of slowing, complexity, and functional connectivity reflect neurodegenerative processes in AD and may facilitate the objectivization of diagnosis and progression. However, they do not demonstrate an added benefit of sLORETA in quantitatively assessing AD severity in routine clinical practice.

Importantly, our results are specific to AD and sLORETA. Therefore, they should not be generalized to other neurological or psychiatric disorders or to other 3D source localization methods without further validation. Finally, these findings do not diminish the value of 3D source localization for visual EEG inspection.

Funding

PRODEM was supported by the Austrian Research Promotion Agency FFG, project no. 827462, including financial contributions by Dr. Grossegger & Drbal GmbH, Vienna, Austria.

Data and code availability statement

The data that support the findings of this study are available from the corresponding author, upon reasonable request. Access to the data will be granted based on the specific requirements and the intended use, subject to approval by the study's authors.

CRediT authorship contribution statement

Wolfgang Frühwirt: Writing – review & editing, Writing – original draft, Visualization, Validation, Software, Project administration, Methodology, Investigation, Formal analysis, Data curation. **Martin Mairhofer:** Writing – original draft, Visualization, Software, Methodology, Investigation, Formal analysis, Data curation. **Andreas Hahn:** Writing – review & editing, Writing – original draft, Validation, Supervision. **Heinrich Garn:** Writing – original draft, Supervision, Software, Methodology, Funding acquisition, Formal analysis, Data curation, Conceptualization. **Markus Waser:** Writing – review & editing, Writing – original draft, Supervision, Software, Methodology, Formal analysis, Data curation, Conceptualization. **Reinhold Schmidt:** Resources, Methodology, Funding acquisition, Conceptualization. **Thomas Benke:** Resources, Methodology, Conceptualization. **Peter Dal-Bianco:** Resources, Methodology, Conceptualization. **Gerhard Ransmayr:** Resources, Methodology, Conceptualization. **Dieter Grossegger:** Writing – original draft, Supervision, Software, Methodology, Investigation, Conceptualization. **Stephen Roberts:** Writing – review & editing, Writing – original draft, Validation, Supervision, Methodology. **Georg Dorffner:** Writing – review & editing, Writing – original draft, Validation, Supervision, Methodology, Conceptualization.

Declaration of competing interest

The authors declare that they have no known competing financial interests or personal relationships that could have appeared to influence the work reported in this paper.

Acknowledgements

We would like to thank Erwin Gabler for his valuable technical contributions.

Supplementary materials

Supplementary material associated with this article can be found, in the online version, at doi:10.1016/j.neuroimage.2025.121144.

References

Akaike, H., 1974. A new look at the statistical model identification. IEEE Trans. Autom. Control 19 (6), 716–723.

Alzheimer's Association, 2017. 2017 Alzheimer's disease facts and figures. Alzheimer's Dement. 13 (4), 325–373.

Andrews-Hanna, J.R., Reidler, J.S., Sepulcre, J., Poulin, R., Buckner, R.L., 2010. Functional-anatomic fractionation of the brain's default network. Neuron 65, 550–562.

Aoki, Y., Takahashi, R., Suzuki, Y., et al., 2023. EEG resting-state networks in Alzheimer's disease associated with clinical symptoms. Sci. Rep. 13 (1), 3964.

Arnold, S.E., Hyman, B.T., Flory, J., et al., 1991. The topographical and neuroanatomical distribution of neurofibrillary tangles and neuritic plaques in the cerebral cortex of patients with Alzheimer's disease. Cereb. Cortex 1 (1), 103–116.

Babiloni, C., Binetti, G., Cassetta, E., Cerboneschi, D., Dal Forno, G., Del Percio, C., et al., 2004. Mapping distributed sources of cortical rhythms in mild Alzheimer's disease. A multicentric EEG study. Neuroimage 22 (1), 57–67.

Babiloni, C., Binetti, G., Cassetta, E., Dal Forno, G., Del Percio, C., Ferreri, F., Rossini, P. M., et al., 2006c. Sources of cortical rhythms change as a function of cognitive impairment in pathological aging: a multicenter study. Clin. Neurophysiol. 117 (2), 252–268.

Babiloni, C., Cassetta, E., Dal Forno, G., Del Percio, C., Ferreri, F., Ferri, R., Rossini, P.M., et al., 2006a. Donepezil effects on sources of cortical rhythms in mild Alzheimer's disease: responders vs. non-responders. Neuroimage 31 (4), 1650–1665.

Babiloni, C., Del Percio, C., Lizio, R., et al., 2016. Classification of single normal and Alzheimer's Disease individuals from cortical sources of resting State EEG rhythms. Front. Neurosci. 10, 47.

Babiloni, C., Frisoni, G., Steriade, M., Bresciani, L., Binetti, G., Del Percio, C., Rossini, P. M., et al., 2006b. Frontal white matter volume and delta EEG sources negatively correlate in awake subjects with mild cognitive impairment and Alzheimer's disease. Clin. Neurophysiol. 117 (5), 1113–1129.

Babiloni, C., Frisoni, G.B., Vecchio, F., Lizio, R., Pievani, M., Cristina, G., et al., 2011. Stability of clinical condition in mild cognitive impairment is related to cortical sources of alpha rhythms: an electroencephalographic study. Hum. Brain Mapp. 32 (11), 1916–1931.

Babiloni, C., Lizio, R., Del Percio, C., Marzano, N., Soricelli, A., Salvatore, E., et al., 2013. Cortical sources of resting state EEG rhythms are sensitive to the progression of early stage Alzheimer's disease. J. Alzheimer's Dis. 34 (4), 1015–1035.

Babiloni, C., Lizio, R., Vecchio, F., Frisoni, G.B., Pievani, M., Geroldi, C., et al., 2010. Reactivity of cortical alpha rhythms to eye opening in mild cognitive impairment and Alzheimer's disease: an EEG study. Journal of Alzheimer's Disease 22 (4), 1047–1064.

Babiloni, C., Lopez, S., Noce, G., et al., 2023. Relationship between default mode network and resting-state electroencephalographic alpha rhythms in cognitively unimpaired seniors and patients with dementia due to Alzheimer's disease. Cereb. Cortex 33 (20), 10514–10527.

Babiloni, C., Triggiani, A.I., Lizio, R., et al., 2017. Classification of single normal and Alzheimer's disease individuals from cortical sources of resting State EEG rhythms. Front. Neurosci. 10, 47.

Benjamini, Y., Hochberg, Y., 1995. Controlling the false discovery rate: a practical and powerful approach to multiple testing. J. R. Stat. Soc. Ser. B (Methodol.) 57 (1), 289–300.

Brett, M., Johnsrude, I.S., Owen, A.M., 2002. The problem of functional localization in the human brain. Nat. Rev. Neurosci. 3 (3), 243–249.

Brillinger, D.R., 1981. Time Series: Data Analysis and Theory. SIAM.

Canuet, L., Tellado, I., Couceiro, V., Fraile, C., Fernandez-Novoa, L., Ishii, R., ... & Cacabelos, R. (2012). Resting-state network disruption and APOE genotype in Alzheimer's disease: a lagged functional connectivity study.

Carrarini, C., Nardulli, C., Titti, L., Iodice, F., Miraglia, F., Vecchio, F., Rossini, P.M., 2024. Neuropsychological and electrophysiological measurements for diagnosis and prediction of dementia: a review on Machine Learning approach. Ageing Res. Rev., 102417

Caso, F., Cursi, M., Magnani, G., Fanelli, G., Falautano, M., Comi, G., et al., 2012. Quantitative EEG and LORETA: valuable tools in discerning FTD from AD? Neurobiol. Aging 33 (10), 2343–2356.

Cecchetti, G., Agosta, F., Basaia, S., et al., 2021. Resting-state electroencephalographic biomarkers of Alzheimer's disease. NeuroImage Clin. 31, 102711.

Cover, T.M., Thomas, J.A., 1991. Entropy, relative entropy and mutual information. Elem. Inf. Theory 2, 1–55.

Dattola, S., La Foresta, F., 2020. An eLORETA longitudinal analysis of resting state EEG rhythms in Alzheimer's disease. Appl. Sci. 10 (16), 5666.

Dauwels, J., Vialatte, F., Cichocki, A., 2010a. Diagnosis of Alzheimer's disease from EEG signals: where are we standing? Curr. Alzheimer Res. 7 (6), 487–505.

Dauwels, J., Vialatte, F., Musha, T., et al., 2010b. A comparative study of synchrony measures for the early diagnosis of Alzheimer's disease based on EEG. Neuroimage 49 (1), 668–693.

Delacourte, A., David, J., Sergeant, N., et al., 1999. The biochemical pathway of neurofibrillary degeneration in aging and Alzheimer's disease. Neurology 52 (6), 1158.

Dickey, D.A., Fuller, W.A., 1979b. Distribution of the estimators for autoregressive time series with a unit root. J. Am. Stat. Assoc. 74 (366a), 427–431.

Dickey, D.A., Fuller, W.A., 1979a. Distribution of the estimators for autoregressive time series with a unit root. J. Am. Stat. Assoc. 74 (366a), 427–431.

Dierks, T., Jelic, V., Pascual-Marqui, R.D., et al., 2003. Spatial pattern of cerebral glucose metabolism (PET) correlates with localization of intracerebral EEG-generators in Alzheimer's disease. Clin. Neurophysiol. 111 (10), 1817–1824.

Draper, N.R., Smith, H., 2014. Applied Regression Analysis. John Wiley & Sons.

Fruehwirt, W., Dorffner, G., Roberts, S., et al., 2019. Associations of event-related brain potentials and Alzheimer's disease severity: a longitudinal study. Prog. Neuro-Psychopharmacol. Biol. Psychiatry 92, 31–38.

Garn, H., Waser, M., Deistler, M., et al., 2014a. Quantitative EEG in Alzheimer's disease: cognitive state, resting state and association with disease severity. Int. J. Psychophysiol. 93 (3), 390–397.

Garn, H., Waser, M., Deistler, M., et al., 2015. Quantitative EEG markers relate to Alzheimer's disease severity in the Prospective Dementia Registry Austria (PRODEM). Clin. Neurophysiol. 126 (3), 505–513.

Garn, H., Waser, M., Deistler, M., Benke, T., Dal-Bianco, P., Ransmayr, G., Schmidt, R., 2014b. Electroencephalographic complexity markers explain neuropsychological test scores in Alzheimer's disease. In: Proceedings of the IEEE-EMBS International Conference on Biomedical and Health Informatics (BHI). IEEE, pp. 496–499.

Gianotti, L.R., Künig, G., Lehmann, D., et al., 2007. Correlation between disease severity and brain electric LORETA tomography in Alzheimer's disease. Clin. Neurophysiol. 118 (1), 186–196.

Granger, C.W., 1969. Investigating causal relations by econometric models and cross-spectral methods. Econom. J. Econom. Soc. 424–438.

Hampel, H., O'Bryant, S.E., Molinuevo, J.L., et al., 2018. Blood-based biomarkers for Alzheimer disease: mapping the road to the clinic. Nat. Rev. Neurol. 14, 639–652.

Hanslmayr, S., Staudigl, T., Fellner, M.C., 2012. Oscillatory power decreases and long-term memory: the information via desynchronization hypothesis. Front. Hum. Neurosci. 6, 74.

Hata, M., Kazui, H., Tanaka, T., et al., 2016. Functional connectivity assessed by resting state EEG correlates with cognitive decline of Alzheimer's disease–an eLORETA study. Clin. Neurophysiol. 127 (2), 1269–1278.

Hotelling, H., 1936. Relations between two sets of variates. Biometrika 28 (3/4), 321–377.

Jensen, O., Mazaheri, A., 2010. Shaping functional architecture by oscillatory alpha activity: gating by inhibition. Front. Hum. Neurosci. 4.

Jeong, J., 2004. EEG dynamics in patients with Alzheimer's disease. Clin. Neurophysiol. 115 (7), 1490–1505.

Klimesch, W., 1999. EEG alpha and theta oscillations reflect cognitive and memory performance: a review and analysis. Brain Res. Rev. 29, 169–195.

Klimesch, W., Doppelmayr, M., Hanslmayr, S., 2006. Upper alpha ERD and absolute power: their meaning for memory performance. Prog. Brain Res. 159, 151–165.

Klimesch, W., Sauseng, P., Hanslmayr, S., 2007. EEG alpha oscillations: the inhibition–timing hypothesis. Brain Res. Rev. 53 (1), 63–88.

Lancaster, J.L., Woldorff, M.G., Parsons, L.M., et al., 2000. Automated Talairach atlas labels for functional brain mapping. Hum. Brain Mapp. 10 (3), 120–131.

Maes, F., Collignon, A., Vandermeulen, D., Marchal, G., Suetens, P., 1997. Multimodality image registration by maximization of mutual information. IEEE Trans. Med. Imaging 16 (2), 187–198.

Maestú, F., Peña, J.M., Garcés, P., González, S., Bajo, R., Bagic, A., et al., 2015. A multicenter study of the early detection of synaptic dysfunction in Mild Cognitive Impairment using magnetoencephalography-derived functional connectivity. NeuroImage Clin. 9, 103–109.

Mazziotta, J., Toga, A., Evans, A., et al., 2001. A probabilistic atlas and reference system for the human brain: international consortium for brain mapping (ICBM). Philos. Trans. R. Soc. Lond. Ser. B Biol. Sci. 356 (1412), 1293–1322.

Mitchell, A.J., 2009. A meta-analysis of the accuracy of the mini-mental state examination in the detection of dementia and mild cognitive impairment. J. Psychiatr. Res. 43 (4), 411–431.

Mulert, C., Jäger, L., Schmitt, R., et al., 2004. Integration of fMRI and simultaneous EEG: towards a comprehensive understanding of localization and time-course of brain activity in target detection. Neuroimage 22 (1), 83–94.

Nishida, K., Yoshimura, M., Isotani, T., et al., 2011. Differences in quantitative EEG between frontotemporal dementia and Alzheimer's disease as revealed by LORETA. Clin. Neurophysiol. 122 (9), 1718–1725.

Oakes, T.R., Pizzagalli, D.A., Hendrick, A.M., et al., 2004. Functional coupling of simultaneous electrical and metabolic activity in the human brain. Hum. Brain Mapp. 21 (4), 257–270.

Palmqvist, S., Schöll, M., Strandberg, O., et al., 2017. Earliest accumulation of β-amyloid occurs within the default-mode network and concurrently affects brain connectivity. Nat. Commun. 8 (1), 1–13.
Park, H.J., Jeong, D.U., Park, K.S., 2002. Automated detection and elimination of periodic ECG artifacts in EEG using the energy interval histogram method. IEEE Trans. Biomed. Eng. 49 (12), 1526–1533.
Pascual-Marqui, R.D., 2002. Standardized low-resolution brain electromagnetic tomography (sLORETA): technical details. Methods Find. Exp. Clin. Pharmacol. 24, 5–12. Suppl D.
Pascual-Marqui R.D., Discrete, 3D distributed, linear imaging methods of electric neuronal activity. Part 1: exact, zero error localization. arXiv preprint arXiv: 0710.3341. 2007.
Pascual-Marqui, R.D., Michel, C.M., Lehmann, D., 1994. Low resolution electromagnetic tomography: a new method for localizing electrical activity in the brain. Int. J. Psychophysiol. 18 (1), 49–65.
Pfurtscheller, G., Aranibar, A., 1977. Event-related cortical desynchronization detected by power measurements of scalp EEG. Electroencephalogr. Clin. Neurophysiol. 42 (6), 817–826.
Pizzagalli, D.A., Oakes, T.R., Davidson, R.J., 2003. Coupling of theta activity and glucose metabolism in the human rostral anterior cingulate cortex: an EEG/PET study of normal and depressed subjects. Psychophysiology 40 (6), 939–949.
Rosenberg, J., Amjad, A., Breeze, P., et al., 1989. The fourier approach to the identification of functional coupling between neuronal spike trains. Prog. Biophys. Mol. Biol. 53 (1), 1–31.
Sadat-Nejad, Y., Beheshti, S., 2021. Efficient high resolution sLORETA in brain source localization. J. Neural Eng. 18 (1), 016013.
Shannon, C.E., 1948. A mathematical theory of communication. Bell Syst. Tech. J. 27 (3), 379–423.
Shannon, C.E., Weaver, W., 1949. The Mathematical Theory of Communication. University of Illinois Press IL, Urbana, IL.
Shim, Y.S., Shin, H.E., 2020. Analysis of neuropsychiatric symptoms in patients with Alzheimer's disease using quantitative EEG and sLORETA. Neurodegener. Dis. 20 (1), 12–19.
Triggiani, A.I., Bevilacqua, V., Brunetti, A., Lizio, R., Tattoli, G., Cassano, F., et al., 2017. Classification of healthy subjects and Alzheimer's disease patients with Dementia from cortical sources of resting state EEG rhythms: a study using artificial neural networks. Front. Neurosci. 10, 604.
Tsallis, C., 1988. Possible generalization of Boltzmann-Gibbs statistics. J. Stat. Phys. 52 (1–2), 479–487.
Valotassiou, V., Papatriantafyllou, J., Sifakis, N., et al., 2015. Clinical evaluation of brain perfusion SPECT with Brodmann areas mapping in early diagnosis of Alzheimer's disease. J. Alzheimer's Dis. 47 (3), 773–785.
Vecchio, F., Miraglia, F., Alù, F., Menna, M., Judica, E., Cotelli, M., Rossini, P.M., 2020. Classification of Alzheimer's disease with respect to physiological aging with innovative EEG biomarkers in a machine learning implementation. J. Alzheimer's Dis. 75 (4), 1253–1261.
Vigneau, M., Beaucousin, V., Hervé, P.Y., et al., 2006. Meta-analyzing left hemisphere language areas: phonology, semantics, and sentence processing. Neuroimage 30 (4), 1414–1432.
Vitacco, D., Brandeis, D., Pascual-Marqui, R., et al., 2002. Correspondence of event-related potential tomography and functional magnetic resonance imaging during language processing. Hum. Brain Mapp. 17 (1), 4–12.
Walker, G.T., 1931. On periodicity in series of related terms. Proc. R. Soc. Lond. Ser. A 131 (818), 518–532. Containing Papers of a Mathematical and Physical Character.
Waser, M., Garn, H., 2013. Removing cardiac interference from the electroencephalogram using a modified Pan-Tompkins algorithm and linear regression. In: Proceedings of the 35th Annual International Conference of the IEEE Engineering in Medicine and Biology Society (EMBC). IEEE, pp. 2028–2031.
Waser, M., Garn, H., Schmidt, R., et al., 2016. Quantifying synchrony patterns in the EEG of Alzheimer's patients with linear and non-linear connectivity markers. J. Neural Eng. 123 (3), 297–316.
Worrell, G.A., Lagerlund, T.D., Sharbrough, F.W., et al., 2000. Localization of the epileptic focus by low-resolution electromagnetic tomography in patients with a lesion demonstrated by MRI. Brain Topogr. 12 (4), 273–282.
Yule, G.U., 1927. VII. On a method of investigating periodicities disturbed series, with special reference to Wolfer's sunspot numbers. Philos. Trans. R. Soc. Lond. Ser. A 226 (636–646), 267–298. Containing Papers of a Mathematical or Physical Character.
Zumsteg, D., Wennberg, R., Treyer, V., et al., 2005. H215O or 13NH3 PET and electromagnetic tomography (LORETA) during partial status epilepticus. Neurology 65 (10), 1657–1660.